Diffusion brazing of Nicrofer 5520 (IN-617) superalloy using an amorphous Ni-Cr-Si-B interlayer: Microstructural characterization and mechanical properties

Ali Nasajpour, Seyyed Ehsan Mirsalehi*, Ali Farzadi

Department of Materials and Metallurgical Engineering, Amirkabir University of Technology (AUT), Hafez Avenue, Tehran, Iran

Abstract

The applicability of the diffusion brazing technique for bonding Nicrofer 5520 superalloy was assessed. The experiments were carried out at 1120 °C for 5, 15, 20, 45, 90, 120, and 240 min holding times using 30 µm thick Ni-7%Cr4.5%Si-3.1%B interlayers. The microstructure, shear strength, and microhardness of the resultant joints were investigated. The results showed that the complete isothermal solidification (CIS) occurred after 20 min-holding time. The (Mo, Cr, Ni, Fe)-rich carbides and (Cr, Mo)-rich borides with various morphologies were observed in the diffusion-affected zone (DAZ). Before CIS, a Ni-rich boride and Ni-rich silicide along with Cr and Mo-rich borides were also detected in the centerline. After CIS, the volume fraction of precipitated phases in the DAZ region was reduced by increasing the holding time. Simultaneously, the chemical composition became more uniform; also, the shear strength of the specimens was improved, and for the 240 min-holding time, it reached about 93 % of that of the base metal.

K e y w o r d s: Nicrofer 5520, diffusion brazing, bonding time, microstructure, mechanical properties

1. Introduction

The superalloys used in the hot sections of gas turbines and aero-engines must have high temperature and cyclic oxidation resistance while combining stress rupture and fatigue strength [1]. Nickel base superalloys are an excellent choice for these applications, and their durability, strength, and surface stability at temperatures up to 85 % of their absolute melting points are very well. Nicrofer 5520 (Ni-22Cr-12Co-9Mo) is primarily a solid solution nickel-base superalloy with superior engineering properties [2]. Because of the excellent features of high-temperature strength and creep resistance, this alloy has been widely used in aerospace, power plants, and chemical industries. In addition, this alloy is extensively used in many reducing and oxidizing environments due to its excellent hot corrosion behavior derived from the simultaneous presence of chromium, aluminum, and molybdenum in the alloy composition [3, 4].

Fusion welding methods are among the most widely used techniques used for Nicrofer 5520 parts. While this alloy has good weldability, it commonly suffers from heat-affected zone (HAZ) cracking before and after post-weld heat treatment. Diffusion brazing is a proper alternative to fusion welding and classical brazing techniques for joining components made of highly sensitive Ni-base superalloys with high joint reliability [5]. Diffusion brazing does not have the common imperfections of fusion welding and provides advantages over classical diffusion bonding as it does not need high pressures and clamping forces. Diffusion brazing also has homogeneous composition profiles and is less sensitive to surface imperfections and gap size fluctuations [6].

In diffusion brazing, the filler metal containing a melting point depressant (MPD) element between the base metal surfaces reduces the diffusion brazing time [7, 8]. The diffusion brazing is accomplished at a temperature between the liquidus of the filler metal and

---

*Corresponding author: tel.: +98 21 64542978; e-mail address: mirsalehi@aut.ac.ir

T a b l e 1. Nominal chemical composition and transformation temperatures of the base metal and filler metal (wt.%) [4]

Element	Cr	Co	Mo	Al	C	Ti	B	Fe	Si	Ni	Solidus temperature ($\degree$C)	Liquidus temperature ($\degree$C)
Nicrofer 5520	23	12	9	1.1	0.6	0.4	0.001	1.5	–	Balance	1330	1380
BNi-2	7	–	–	–	0.06	–	3.1	–	4.5	Balance	971	999

the solidus of the base metal. The process has three main stages [8]: dissolution of the base metal, isothermal solidification, and homogenization of the diffusion braze area. Basically, the interlayer melts and fills the joint clearance by holding specimens at the diffusion brazing temperature, and dissolution occurs. The MPD element diffuses into the base metal in isothermal solidification [9, 10]. After completing isothermal solidification, no liquid phases would remain in the diffusion brazed area. The homogenization step aims to obtain similar microstructures and chemical compositions in all areas. The diffusion brazing parts should be held for a long enough time to allow isothermal solidification to complete and avoid the generation of brittle phases in the middle of the bonding gap. The diffusion brazing process aims to achieve the highest similarity of the joint's microstructural characteristics and distribution of elements to those of the base metal [5]. Therefore, selecting the proper time and temperature in the diffusion brazing cycle is important in attaining suitable joints comparable with the base metal in terms of microstructure and mechanical properties [11, 12].

In the present study, the diffusion brazing of Nicrofer 5520 using Ni-7%Cr-4.5%Si-3.1%B interlayer was investigated. The objective of the present research was to investigate the influence of holding time on the metallurgical structure, shear strength, and microhardness of these diffusion brazing joints. Finally, it was tried to homogenize the chemical composition and microstructure of the joint area by employing longer holding times at the diffusion brazing temperature after isothermal solidification.

2. Experimental procedure

The hot-rolled Nicrofer 5520 superalloy is used as base metal, with a thickness of 10 mm. The BNi-2 nickel-based filler metals with a thickness of 30 μm were used. The chemical composition and the transformation temperatures of the filler metals and the base metal are given in Table 1 [4].

Initially, Nicrofer 5520 superalloy sheet surfaces with the aim of creating the same thickness in all areas of the sheet and also creating a smooth surface of 0.8 Ra were prepared by the magnetic grinding process. Then, the specimens were extracted from the sheet in a cylindrical shape with a diameter of 5 mm and a

length of 5 mm using the wire cut method according to the BAHR Dilatometer Thermo Analysis standard.

The surface of the specimens was ground up to 2000 grit sandpaper to achieve the desired level of smoothness and remove the oxide layer. Then, it was cleaned with acetone before the diffusion brazing operation. The interlayer foils were cut using a punching machine with a dimension of 5 mm in diameter. Before placing the foils between the two test specimens, they were also cleaned with acetone to remove any contamination. Then, between the two base metal pieces, an interlayer was attached.

A dilatometer device (DIL805A/D) was used for the first time in the world to perform the diffusion brazing process. In a dilatometer, two specimens are placed between the punches of the device in such a way that the amount of vertical pressure applied to them can be adjusted to the meticulous, with an accuracy of a tenth newton, the specimens are placed inside the induction coils, and the temperature is measured with an accuracy of $0.05\,\degree$C. With this device, the amount of vacuum reaches 1×10^{-5} Torr. Figures 1a,b show the encasement of a dilatometer device and the process chamber, respectively.

The eutectic temperature of the binary Ni-B alloy was reported to be in the range of 1080–1140$\degree$C [13]. Therefore, the temperature of 1120$\degree$C, which is inside the range of 1080–1140$\degree$C, was selected. Therefore, the diffusion brazing was performed at 1120$\degree$C with 5, 15, 20, 45, 90, 120, and 240 min holding times. The chosen temperatures were higher than the liquidus temperatures of the selected interlayer (Table 1). The diffusion brazing cycle was applied at $15\,\degree\text{C}\,\text{min}^{-1}$ heating rate and $5\,\degree\text{C}\,\text{min}^{-1}$ cooling rate. The applied pressure on the specimens was selected as 0.2 MPa and applied by the device; this amount of pressure was selected to be the same for all specimens.

The optical and electron microscopes were used to study the microstructure of the diffusion braze joint areas. The specimens were kept in Killing's etching solution for about 2.5 min after sanding and polishing for microstructural studies. The study of the microstructure and the chemical composition distribution was carried out by SERON ALS2300 scanning electron microscope (SEM), and HITACHI UHR SU9000 field emission scanning electron microscope (FESEM) outfitted with an energy dispersive X-ray spectrometer (EDS). A Shimadzu HydroHITS-T10 tensile machine was used in load control mode employing a prepared
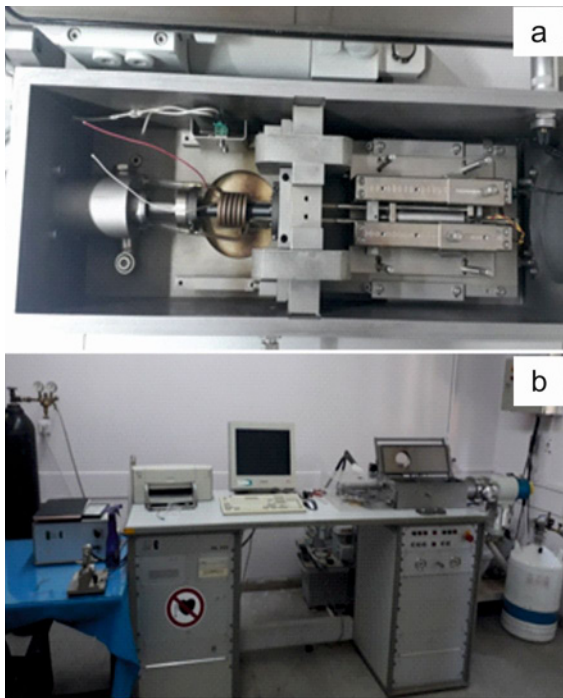
Fig. 1. (a) Dilatometer device and (b) process chamber.
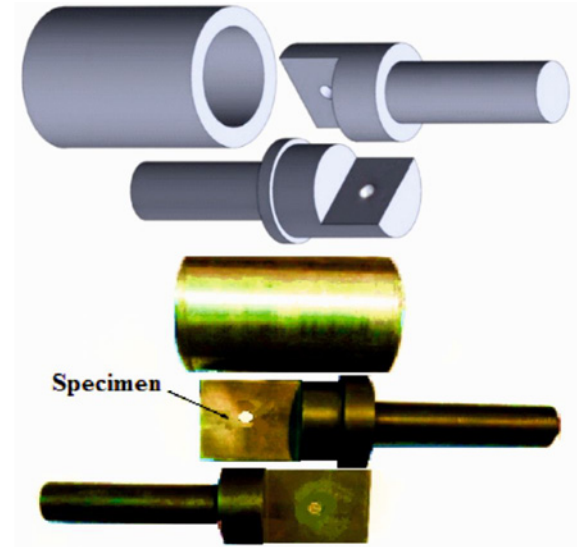
Fig. 2. The shear fixture for performing the shear strength test.
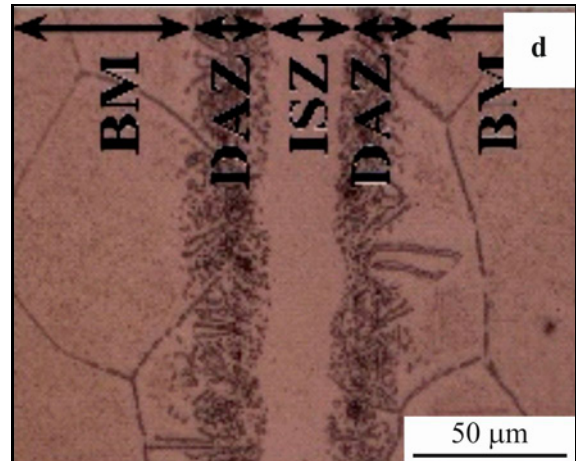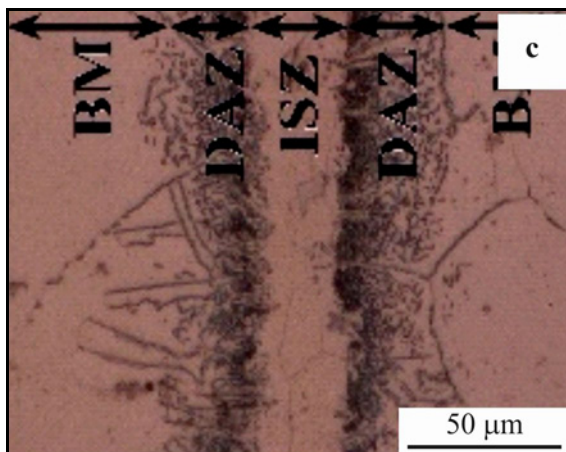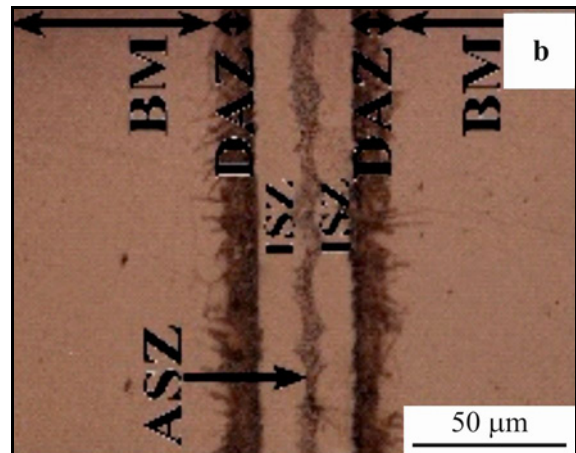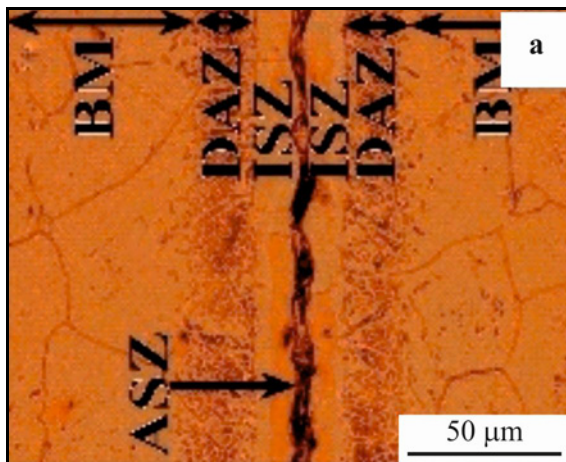
Fig. 3a–d. The diffusion brazing areas (ISZ), (DAZ), and (ASZ) for the diffusion brazed specimens by (a) 5 min, (b) 15 min, (c) 20 min, (d) 45 min holding time.
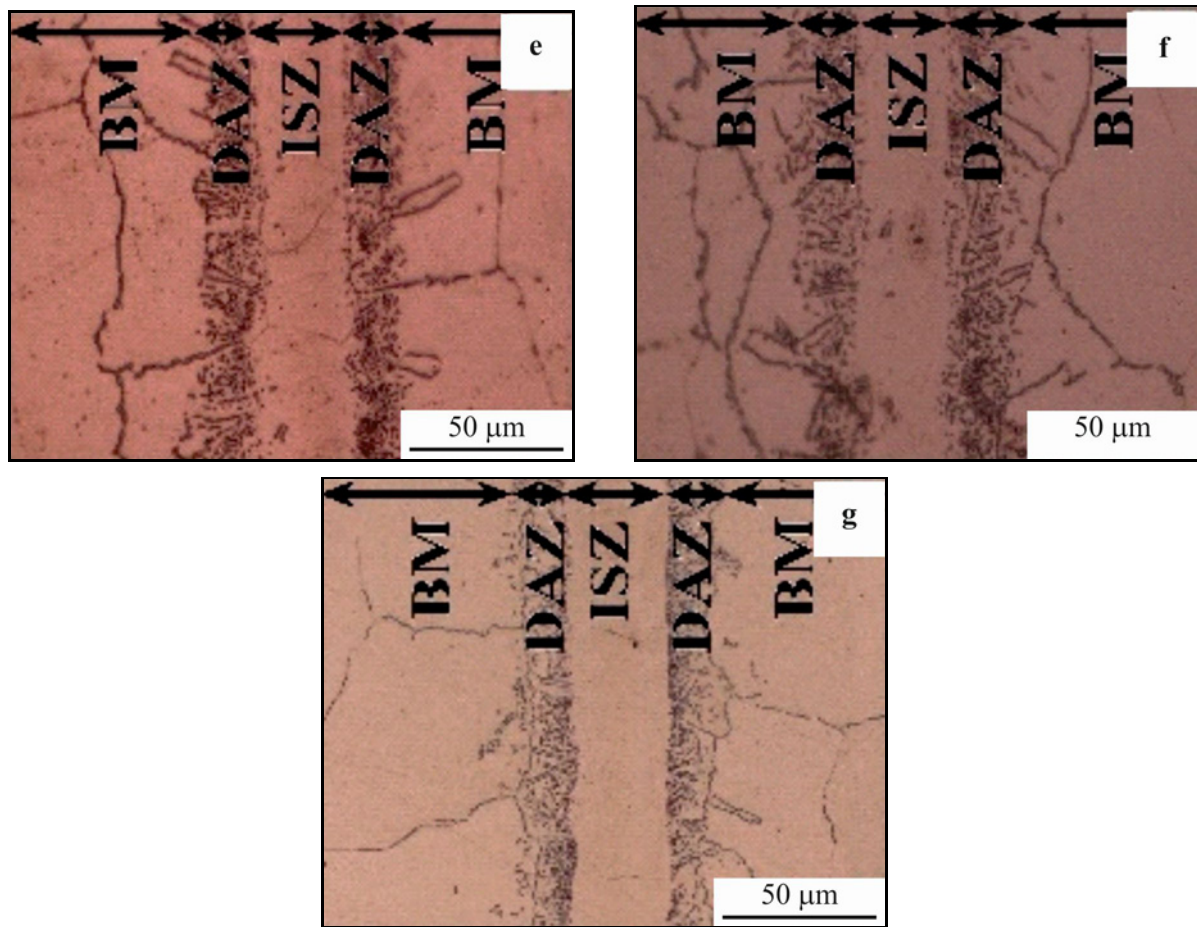
Fig. 3e–g. The diffusion brazing areas (ISZ), (DAZ), and (ASZ) for the diffusion brazed specimens by (e) 90 min, (f) 120 min, and (g) 240 min holding time.

fixture (as shown in Fig. 2) to evaluate the shear strength, displacement, and toughness according to ASTM D1002-05 [13]. Figure 2 shows the fixture used for performing the shear strength test. All specimens were tested by a Matsuzava MMT Vickers micro-hardness test machine in the interlayer and diffusion zone according to ASTM E384-11 [14] under a load of 0.196 N for a resting time of 15 s.

3. Results and discussion

3.1. Optical microscopy

In this study, the diffusion brazing of Nicrofer 5520 was performed using a BNi-2 interlayer at 5 to 240 min holding times. Figure 3 shows the diffusion brazing area, including the isothermal solidification zone (ISZ) and diffusion affected zone (DAZ) for all seven specimens. As shown in Fig. 3, the 5 min holding time was insufficient to complete the isothermal solidification process and was not enough to completely remove the liquid phase. As a result, the athermal solidification zone (ASZ) in the center of the interlayer is formed after cooling the specimens. The ASZ phase has a thickness of one-third of the bonding region ($\sim 7\,\mu m$) and remains in the middle of the bonding area. In the following, by increasing the holding time from 5 to 15 min, the thickness of the ASZ layer decreased so that the result of increasing the holding time to 20 min is the complete elimination of the ASZ phase, and the isothermal solidification process has been completed. The diffusion affected zone (DAZ) on both sides of the interlayer consists of the non-dissolved carbides, boride, and silicide precipitates that were affected by diffused elements from the interlayer to the base metal.

3.2. Scanning Electron Microscopy

The EDS line scan analysis was performed at 5, 20, and 240 minutes from base metals and bonding gap. Figures 4–6 show the results of the EDS line scan in a different zone of bonding areas (ASZ, ISZ, DAZ, and BM). To verify the obtained results of the EDS line scan analysis across in width of the bonding area and in order to investigate the changes in the concentration of elements by increasing the holding time, the EDS line scan was performed for the 5, 20, and

T a b l e 2. The average EDS analysis results for locations shown in Fig. 7

	A	B	C	D	E	F
	Average (wt.%)	Average (wt.%)	Average (wt.%)	Average (wt.%)	Average (wt.%)	Average (wt.%)
Ni	35.4	65.7	36.2	41.1	46.5	51.2
Cr	12.3	5.7	15.6	18.3	20.5	22.8
Mo	7.5	2.4	8.2	8.4	8.5	8.9
Co	1.4	2.6	9.4	10.2	10.8	11.5
Si	3.1	4.3	2.8	1.8	1.1	0.4
B	2.9	1.1	0.3	–	–	–
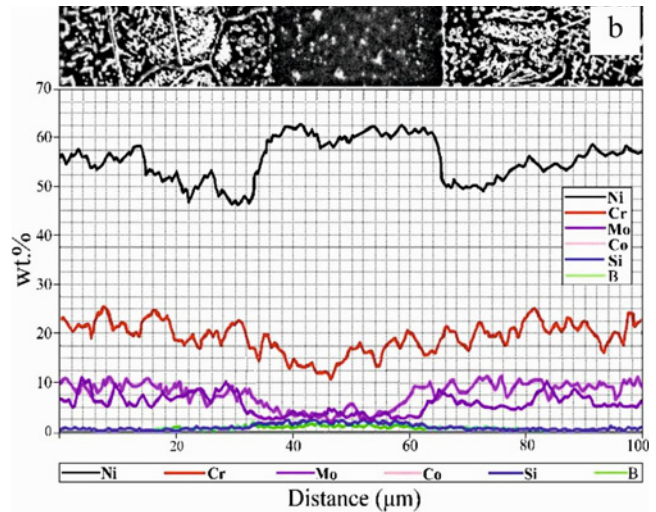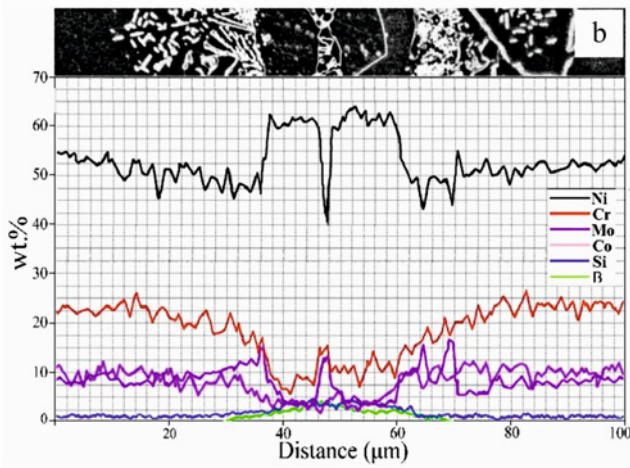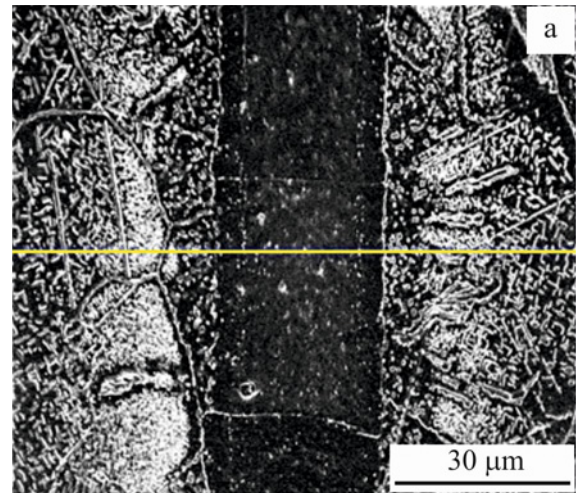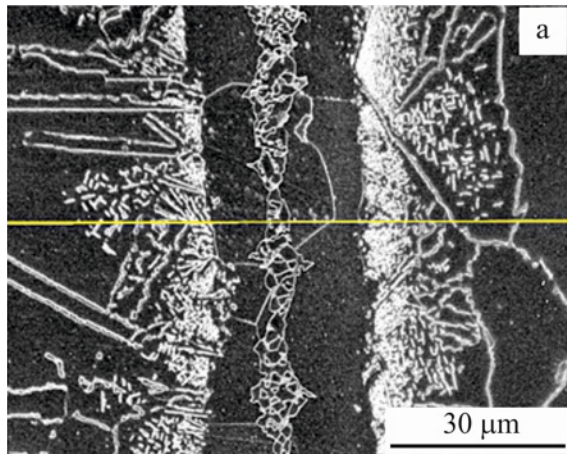
Fig. 4. (a) The SEM micrograph of the 5 min diffusion brazed specimen and (b) the results of the EDS line scan for the 5 min holding time specimen.

Fig. 5. (a) The SEM micrograph of the 20 min diffusion brazed specimen and (b) the results of the EDS line scan for the 20 min holding time specimen.

240 min holding time specimens in 5 regions in parallel with the bonding gap. Figures 7–9 illustrate changes in the concentration of elements in parallel with the bonding gap. The EDS line scan was selected along the A line in the center of the interlayer to investigate changes in the concentration of elements at the farthest place from the base metal, and the EDS line

scan along with line C at a distance of ∼ 15 μm from line A and in accordance with the boundary between the base metal and the interlayer was selected; the EDS line scan along line B was considered to study the concentration changes between the lines A and C. In the following, the EDS line scan along with lines D, E, and F at a distance of ∼ 10, 20, and 30 μm from

Table 3. The average EDS analysis results for locations shown in Fig. 8

	A	B	C	D	E	F
	Average (wt.%)	Average (wt.%)	Average (wt.%)	Average (wt.%)	Average (wt.%)	Average (wt.%)
Ni	59.7	63.2	39.8	42.6	48.3	52.2
Cr	12.4	11.9	17.4	19.6	20.6	21.9
Mo	4.2	3.8	7.8	8.2	8.8	9.2
Co	2.3	3.1	9.2	9.9	10.5	11.8
Si	3.7	3.9	2.6	2.1	1.7	1.2
B	2.4	1.8	1.3	0.9	0.3	–
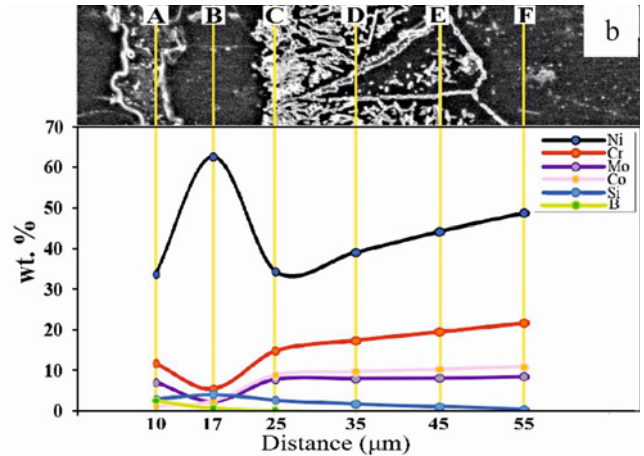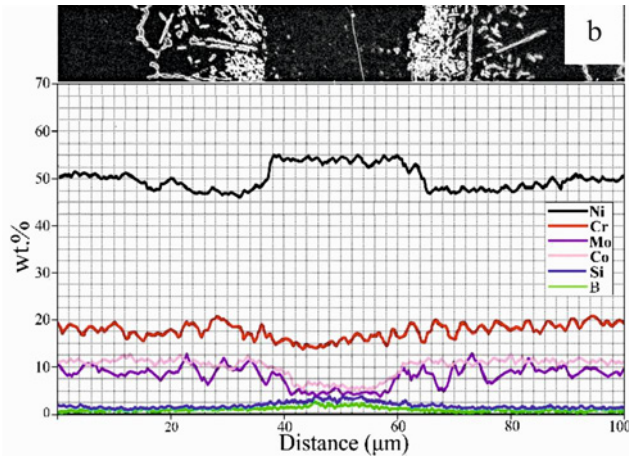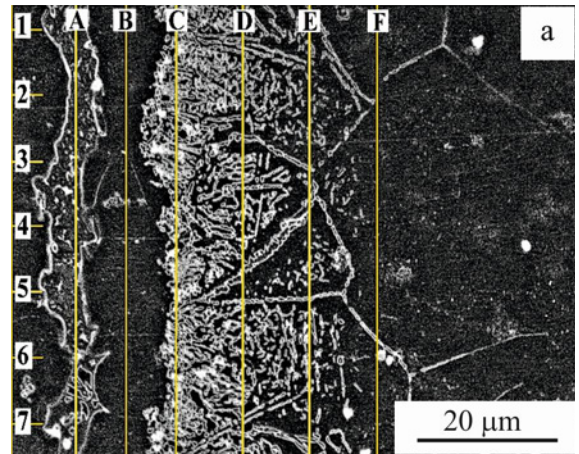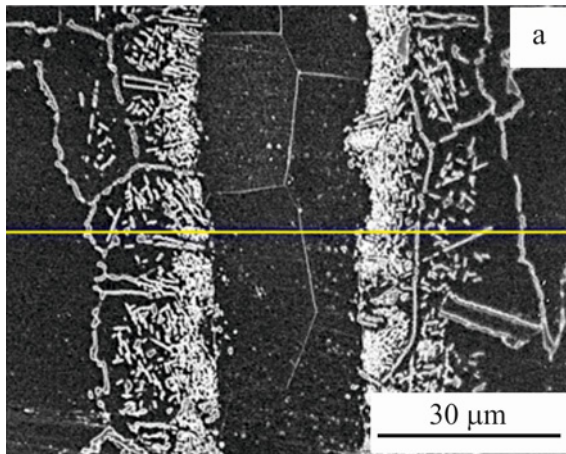
Fig. 6. (a) The SEM micrograph of the 240 min diffusion brazed specimen and (b) the results of the EDS line scan for the 240 min holding time specimen.

Fig. 7. (a) The SEM micrograph of the 5 min diffusion brazed specimen and (b) the results of the EDS line scan in parallel with a bond gap for the 5 min holding time specimen.

line C, respectively, was considered. Tables 2–4 show the chemical composition of the elements Cr, Si, Mo, Co, B, and Ni along with lines A, B, C, D, E, and F for diffusion brazed specimens with a holding time of 5, 20, and 240 min.

In low holding time, due to the insufficient time for completing MPD elements diffusion and equally the lack of base metal elements diffusion to inter-

layer and dissolution in it (according to Figs. 4 and 7 and Table 2), the distribution of alloying elements between the three diffusion brazing zones is not uniform. Shamsabadi et al. [15, 16] have reported the same effect on the diffusion brazing of IN738/ MBF20/IN718. The 5 min holding time specimen is an example of the isothermal solidification step not being completed, and the eutectic phase is seen at the center of the bonding

T a b l e 4. The average EDS analysis results for locations shown in Fig. 9

	A	B	C	D	E	F
	Average (wt.%)	Average (wt.%)	Average (wt.%)	Average (wt.%)	Average (wt.%)	Average (wt.%)
Ni	53.5	55.4	45.6	47.8	49.4	53.2
Cr	13.9	15.1	18.4	20.3	21.7	21.6
Mo	3.9	3.7	8.8	7.4	8.2	8.9
Co	3.5	3.3	8.9	9.6	10.3	11.5
Si	3.1	3.4	2.9	2. 5	2.1	1.8
B	1.6	1.3	1.1	0.9	0.7	0.7

T a b l e 5. Chemical composition (at.%) of the particles on the FESEM backscattered electron image of the bonded area in the 45 min holding time specimen (Fig. 11)

Element	Cr	Co	Mo	C	B	Fe	Si	Ni	Probable phases
A	21.4	0.37	20.6	1.69	48.83	3.67	0.21	19.84	$(Ni,Mo,Cr)B$
B	26.31	0.68	32.24	12.11	0.93	9.94	0.02	17.12	$(Ni,Mo,Cr,Fe)_6C$
C	39.63	0.84	26.88	18.97	1.18	7.23	0.04	5.86	$(Ni,Mo,Cr,Fe)_{23}C_6$

T a b l e 6. Chemical composition (at.%) of the particles on the FESEM backscattered electron image of the bonded area in the 240 min holding time specimen (Fig. 12)

Element	Cr	Co	Mo	C	B	Fe	Si	Ni	Probable phases
A	25.69	0.23	20.95	1.49	45.26	3.52	0.03	3.25	$(Mo,Cr)B$
B	44.74	0.63	0.08	1.73	51.41	1.32	0.05	0.97	$Cr B$
C	3.65	0.14	0.06	1.96	24.52	1.63	0.03	66.46	Ni_3B
D	25.34	0.74	35.23	14.16	0.67	9.32	0.06	16.24	$(Ni,Mo,Cr,Fe)_6C$

gap. As shown in Figs. 4 and 7 and using evidence obtained from Table 2, the EDS line scan in this specimen indicates the accumulation and high percentage of Cr, Si, B, and Mo in the center of the bonding gap (SAZ phase). Because the amount of Ni in the interlayer is about 60 % higher than that in the base metal, and despite the accumulation of elements such as Ni, Cr, Mo, and B, there is a possibility of boride phases formation, so the analysis of the EDS in Fig. 10 is performed by the presence of three-type boride phases. By moving away from the SAZ phase and moving towards the base metal, the Cr percentage decreases sharply, and as we get closer to the base metal, the Cr percentage increases (there is 23 % Cr in the base metal and 7 % Cr in the interlayer). The percentage of the Si element decreases by moving towards the base metal with a gentle slope. The small Mo element accumulation can be seen in the SAZ phase, and intense Mo element accumulation in the DAZ phase. The value of this element inside the interlayer is insignificant and can only be seen in the center of the bonding gap by a minor amount (SAZ phase). Co element is also very small in the interlayer and has no accumulation in the SAZ region.

The diffusion is the base of isothermal solidification phenomena in which increasing holding times made more opportunities for boron atoms to diffuse toward the base metal leading to a diminution in the ASZ zone width. In contrast, the DAZ width incremented with longer holding time, and by following holding time, the DAZ width diminished. Ojo et al. [17], in their work on the diffusion brazing of IN-738, have also reported the reduction of ASZ width in accordance with the increment in the holding time. Figures 5 and 8 show the results of the EDS line scan of the specimen brazed for 20 min holding time. In the 20 min holding time specimen, the isothermal solidification is completed, and the precipitated phase is not seen in the center of the bonding gap. The remarkable point about the EDS line scan analysis of this specimen is the greater uniformity of elements in the width of the interlayer than the 5 min holding time specimen. The intense accumulation of elements in the interlayer is not seen in such a way that the Cr element has a uniform distribution across the width of the interlayer, but its value is still less than the chromium percentage in the base metal, and only a small accumulation of this element can be seen in the DAZ phase. The Mo element also

has a uniform distribution in the width of the interlayer, but a large accumulation of this element can be seen in the DAZ region. The Si element distribution is not uniform in the width of the interlayer, and a high Si concentration in the center of the interlayer exists, but the non-uniformity of this element is much less than for the specimen with a 5 min holding time. As shown in Fig. 8, by moving towards the base metal, the concentration of this element decreases, and there is no accumulation of this element within the DAZ region. The amount of Co element in the interlayer is still very small and has not accumulated in any area. Factually, the isothermal solidification accomplishes at a constant temperature known as diffusion brazing temperature. The B element distribution gets uniformly than the 5 min holding time specimen, but the boron diffusion depth in base metal increased. When the holding time is sufficient, the whole liquid phase will be solidified isothermally, and the disappearance of the residual liquid occurs; as a result, eutectic compounds in the center of the interlayer will disappear. Figure 10 shows the ASZ, ISZ, and DAZ of the 15 min holding time specimen. The ASZ zone is performed from borides and silicide precipitates, and boride and carbide particles are found in the DAZ zone. Various studies have reported the formation of such phases in the ASZ and DAZ zones in different nickel-based superalloys [18–20].

Figures 6 and 9 show the results of the EDS line scan in the 240 min holding time specimen, the holding time was so high that we saw a more intense diffusion rate of the elements, and the chemical composition of the interlayer achieved a very high uniformity with the base metal. The element distribution is in such a way that the Cr element is not only uniform in the interlayer but also the percentage of the Cr element is close to its percentage inside the base metal. Despite the relative uniformity of the Cr element within the interlayer, there is a small accumulation of Cr element in the DAZ phase; this accumulation rate decreased compared to the 20 min holding time specimen. Changes in the concentration of the Mo element have similar conditions to the Cr element, and at the same time, the percentage of this element in the interlayer increased, and its accumulation in the DAZ region was reduced. The concentration distribution of the Si element is uniform across the interlayer, and a small accumulation of this element can be seen in the DAZ region. The concentration of Co in the interlayer increased, and a small accumulation of this element was also seen in the DAZ region.

During the diffusion brazing process, due to the diffusion of elements from the interlayer to the base metal and from the base metal to the interlayer (depending on the concentration of the element in the base metal and the interlayer), changes in the concentration and formation of new phases can be seen.
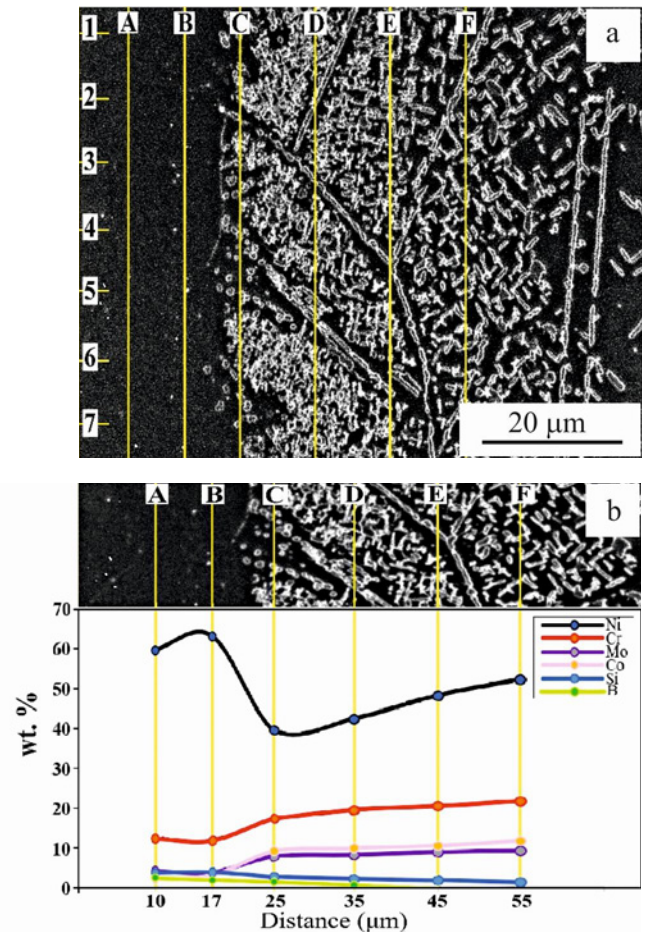
Fig. 8. (a) The SEM micrograph of the 20 min diffusion brazed specimen and (b) the results of the EDS line scan in parallel with a bond gap for the 20 min holding time specimen.

The results in Table 7 indicate that by increasing the bonding time, the concentration of all elements in the width of the interlayer has become more uniform, and their concentration is closer to the chemical composition of base metal. The concentration of elements in the DAZ region before the completion of isothermal solidification (despite the eutectic phase in the bonding center) is low, and elements such as Cr, Si, Mo, and Co have low accumulation in the DAZ region. From 5 to 20 min holding time, the concentration of these elements in this region increased, but by completing the isothermal solidification from 20 min onwards, and with increasing holding time, the concentration of these elements in the DAZ area decreased. By increasing the holding time, the concentration of Cr, Mo, and Co elements in the interlayer increased, and conversely, the concentration of Si element in the interlayer decreased, and its accumulation increased in the DAZ region. Gale and Wallach [13] propounded a mechanism for microstructural development of the

T a b l e 7. The volume fraction of precipitated phases in the DAZ region for 5 to 240 min holding time specimens

Specimen	5 min	15 min	20 min	45 min	90 min	120 min	240 min
DAZ precipitated phases volume fraction	26.4 %	37.3 %	45.8 %	38.5 %	31.3 %	20.6 %	15.4 %
ASZ phases volume fraction	48.9 %	37.4 %	–	–	–	–	–
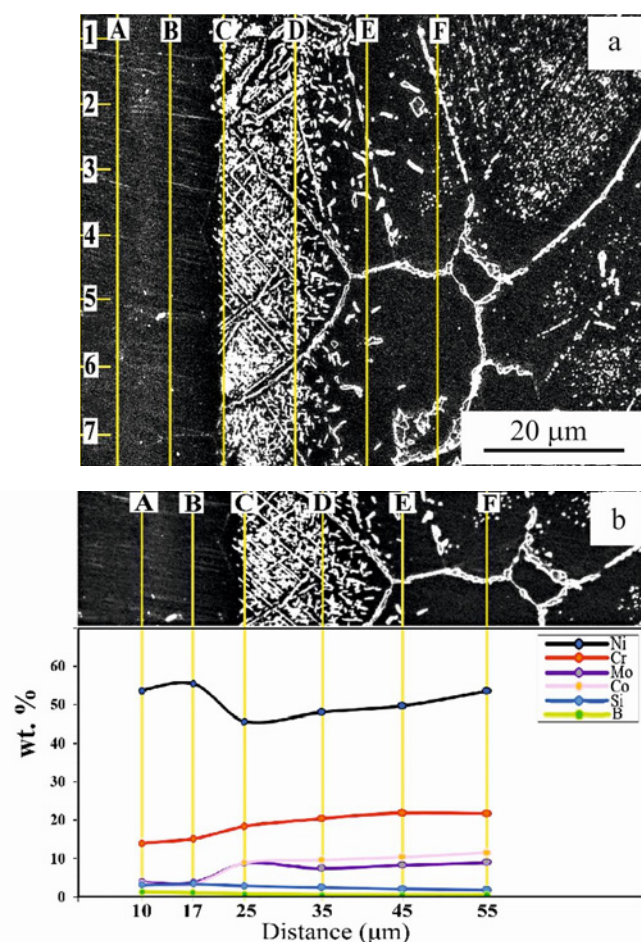
Fig. 9. (a) The SEM micrograph of the 240 min diffusion brazed specimen and (b) the results of the EDS line scan in parallel with a bond gap for the 240 min holding time specimen.

pure nickel diffusion brazing process using a ternary Ni-Si-B interlayer. They reported that the diffusion brazing with the temperature above the binary Ni-B eutectic (1150 °C) has a significantly less number of boride precipitates in DAZ than the temperature below the binary Ni-B eutectic temperature (1065 °C). In the Malekan et al. [21] regarding Hastelloy X, diffusion brazing process with the temperature between the binary Ni-B eutectic (1110 °C) reported that the density of (Cr, Mo)-rich borides in the DAZ of the specimen diffusion brazed at 1110 °C is much higher than that in specimens diffusion brazed at 1070 and 1160 °C.

The uniformity rate of concentration of Cr, Mo, and Co elements in the interlayer varies depending on the diffusion coefficient of the element, as well as the difference and concentration gradient between the intermediate layer and the base metal. As shown in Fig. 3 and Table 7, after completing the isothermal solidification with increasing time, the volume percentage of precipitated phases in the DAZ region decreased, and in the 240 min holding time specimen was removed. The results of the EDS line scan confirm the same so that by increasing the time and simultaneously increasing the uniformity of the concentration of elements in the interlayer and approaching the concentration of elements in the interlayer to the chemical composition of base metal, the concentration of elements in the DAZ region was also reduced. Figure 10a illustrates the SEM micrograph of the diffusion brazed specimen at 15 min and shows different zones in the solidified area by FESEM backscattered electron image (Figs. 10b,c). As can be seen, eutectic products in the centerline of the bond contain A: Ni-rich boride, B: Ni-rich silicide, C: Mo-rich boride, and D: Cr-rich boride. In the DAZ zone, formed phases contain products such as E and F: (Mo, Cr, Ni, Fe)-rich carbides and G: Cr-Mo-rich borides. The solidification sequence during diffusion brazing of the Nicrofer 5520 superalloy with 35-μm-thick interlayer at 1120 °C for 15 min can be elucidated according to the distribution coefficient of the elements and the Ni-Si-B ternary phase diagram [22, 23]. Initially, due to the enrichment of the residual liquid in elements with k values less than unity, the γ solid solution phase solidifies from the solid-liquid. Therefore, the low partition coefficient of B in Ni (0.3 at.%) and Ni in B (~ 0.008) and the low solubility of B in Ni cause occasional rejection of B into the residual liquid [22, 23]. In this situation, the formation of the Ni_3B phase via a eutectic reaction results from the enrichment of the remaining liquid with B. In the following, the formation of the Ni-Si eutectic phase close to the Ni-rich boride results from the dissolution of Si into the remaining liquid. According to Fig. 10, the DAZ was composed of considerable secondary precipitates as (Mo, Cr, Ni, Fe)-rich carbides with various morphologies in grain boundaries and intergranular, and also was composed of Cr-Mo-rich borides in the close of interlayer and base metal boundary [24, 25]. These precipitates formed where the concentration of B close to the junction was high due to exceeded B solubility in the base metal. Also,
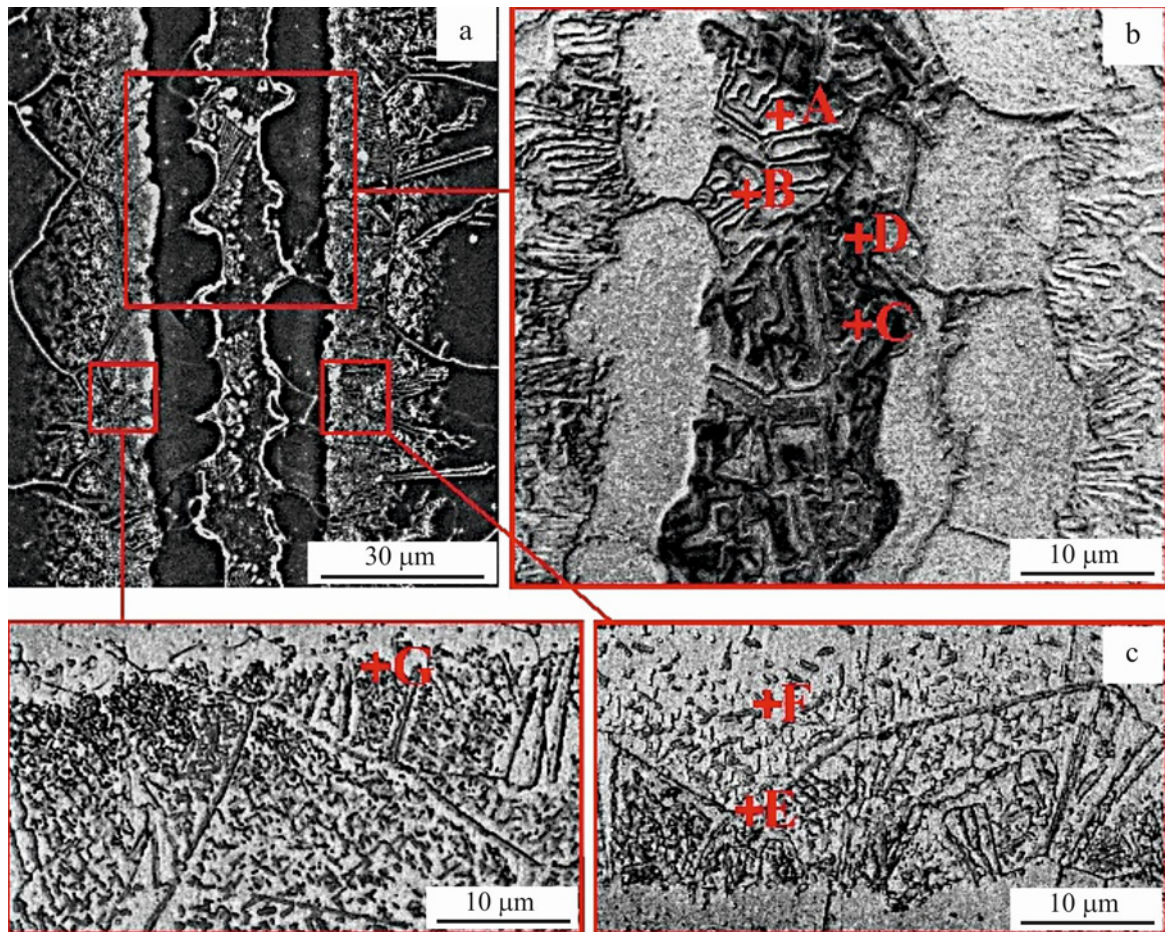
Fig. 10 The SEM micrograph of the diffusion brazed specimen at 15 min: (a) SEM image showing different zones in the solidified area, (b) FESEM backscattered electron image of the solidified zone, and the higher magnification in the eutectic products in the centerline of the bond A: Ni-rich boride, B: Ni-rich silicide, C: Mo-rich boride, D: Cr-rich boride, (c) FESEM backscattered electron image of the solidified zone, and the higher magnification in DAZ products E and F: (Mo, Cr, Ni, Fe)-rich carbide and G: Cr-Mo-rich borides.

in this region, the high reactivity of Mo and Cr with B promotes the formation of Cr-Mo-rich boride precipitates [26]. The chemical compositions (at.%) of the particles on the fracture surfaces of the specimens in Tables 9 and 10 confirm the formation of composed (Mo, Cr)-rich borides and (Mo, Cr, Ni, Fe)-rich carbides in the DAZ zone and Ni-rich boride, Ni-rich silicide, Mo-rich boride, Cr-rich boride in the ASZ zone as shown in Fig. 10 [27].

The boride density decreased with increasing holding time. Zhang et al. [28] studied the precipitation and evolution of borides in the DAZ of Mar-M-247 diffusion brazed joints. They found that two types of carbo-borides and three types of borides precipitated in the DAZ were most likely M23(C, B)6, M6(C, B), M3B2, granular M5B3, and acicular M5B3, respectively. In another study conducted by Liu et al. [29] on Mar-M-247 Ni-based superalloy, it was perceived that after complete isothermal solidification, the microhardness of the joints was more homogeneous. The microstructure and mechanical properties of diffusion

brazed GTD-111 using MBF-20 interlayer were studied by Amiri et al. [30]. The diffusion of the MPD elements from the interlayer to the base metal at the diffusion brazing temperature becomes greater and get intensified when the amount of the element in the ISZ is higher than its solubility limit in the base metal, so, as a result, the boride areas with needle-like, cubic shapes, and grain boundary shapes form close to the bonding interface (DAZ). Researchers presented precipitation of the borides in the DAZ zone in many studies on the IN-738 LC and IN-718 superalloys [26, 31].

The FESEM backscattered electron image of the 45 min holding time specimen is illustrated in Fig. 11. The FESEM-EDS chemical analysis of phases A, B, and C identified the presence of (Ni-Cr-Mo)-rich boride dissolved phases in point A, MC6 carbide type in point B, and M23C6 carbide in point C.

Figure 12 illustrates the FESEM backscattered electron image of the 240 min holding time specimen. The FESEM-EDS chemical analysis of A, B, C, and D
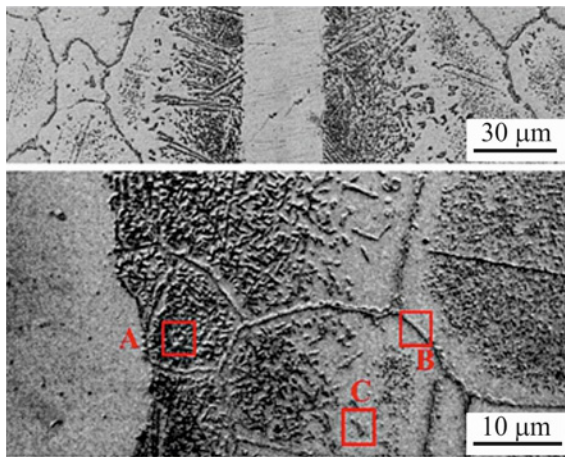
Fig. 11. The FESEM backscattered electron image of the bonded area in the 45 min holding time specimen with two magnifications. According to FESEM-EDS chemical analysis, phases A, B, and C, indicated by the red square, were (Ni-Cr-Mo)-rich boride MC6 and M23C6, respectively.
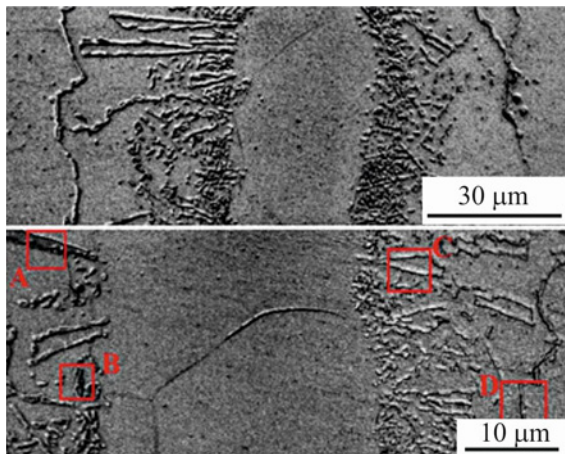
Fig. 12. The FESEM backscattered electron image of the joint area in the 240 min holding time specimen with two magnifications. According to FESEM-EDS chemical analysis, phases A, B, C, D, and E, indicated by the red square, were (Cr, Mo)-rich boride, Cr-rich boride, Ni-rich boride, and (Mo, Cr, Ni, Fe)-carbide, respectively.

Fig. 13. The FESEM backscattered electron image of the 45 min holding time specimen used for measuring the volume fraction of precipitated phases by MIP software.

phases identified the presence of (Cr-Mo)-rich boride dissolved phases in A square, Cr-rich boride in B square, Ni-rich boride in C square, and M6C carbide in D square.

This study used MIP software to calculate the volume fraction of non-dissolved precipitated phases in the DAZ zone. The FESEM backscattered electron image of the 45 min holding time specimen shown in Fig. 13 is a showcase used for measuring phase volume fraction by MIP software. This image is an example of the FESEM backscattered electron images used to calculate the volume fraction of precipitated phases

in the DAZ region. Three images are used to calculate the volume fraction of each specimen, and the obtained number is the average of three-volume fractions extracted from three images for each specimen. Table 7 indicates the volume fraction of precipitated phases in the specimens (DAZ region and ASZ region) for 5 to 240 min holding time using MIP software. As shown in Fig. 13 and Table 7, with increasing time from 20 to 240 min, the width, density, and volume fraction of the DAZ phase decreased due to the dissolution of precipitated phases; but the addition of DAZ and ASZ phases' volume fraction continuously decreased by uprising holding time from 20 min (completion time of the isothermal solidification process) to 240 min, the volume fraction of phases in the DAZ region decreased [32]. The cause of such phenomenon is a created variation due to diffusion over the time of the diffusion brazing. Indeed, at the beginning and in the 5 min holding time specimen, MPD elements did not have the opportunity to diffuse into the base metal, and as a result, a smaller volume fraction of precipitated phases DAZ zone was formed [21, 32]. With increasing holding time up to 15 min, the diffusion rate increased, and at the same time, in this specimen, the volume fraction of phases in the ASZ zone decreased, and the DAZ zone increased. This increase in the volume fraction of the DAZ phase, up to 20 min, reached its maximum value due to the ASZ phase removal and increasing the diffusion of MPD elements [33]. By increasing the holding time beyond 20 min, the volume fraction of the DAZ phase did not increase. The greater diffusion of MPD elements in the depth of the base metal did not increase the DAZ phase [19, 34]. As shown in Fig. 3, with increasing time from 20 to 240 min, the width and density of the DAZ phase decreased due to the dissolution of precipitated phases.
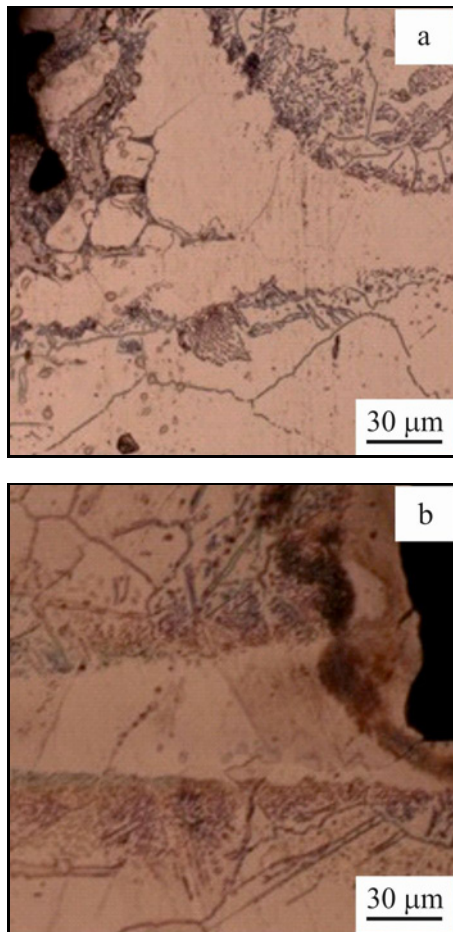
Fig. 14. Edges of the base metals where bonding is not completed: (a) left side of the specimen and (b) right side of the specimen.

3.3. Shear strength testing

Figure 14 shows the bonding edges for a brazed joint. At the distance of 50 μm from the edges of the specimen, no connection was observed. Therefore, it is necessary to remove these edges before performing the shear strength test so that no error occurs in the results. In this regard, grinding was carried out by a peeling machine on the specimens, and the diameter of specimens was reduced from 5 to 4.48 mm.

First, the shear strength of unbounded Nicrofer 5520 superalloy base metal was examined, and the strength of ∼ 690 MPa was obtained. Then, the shear strength of the diffusion brazed specimens was investigated. The shear strength diagram of the given diffusion brazed specimens with holding times of 5, 15, 20, 45, 90, 120, and 240 min is shown in Fig. 15. As shown
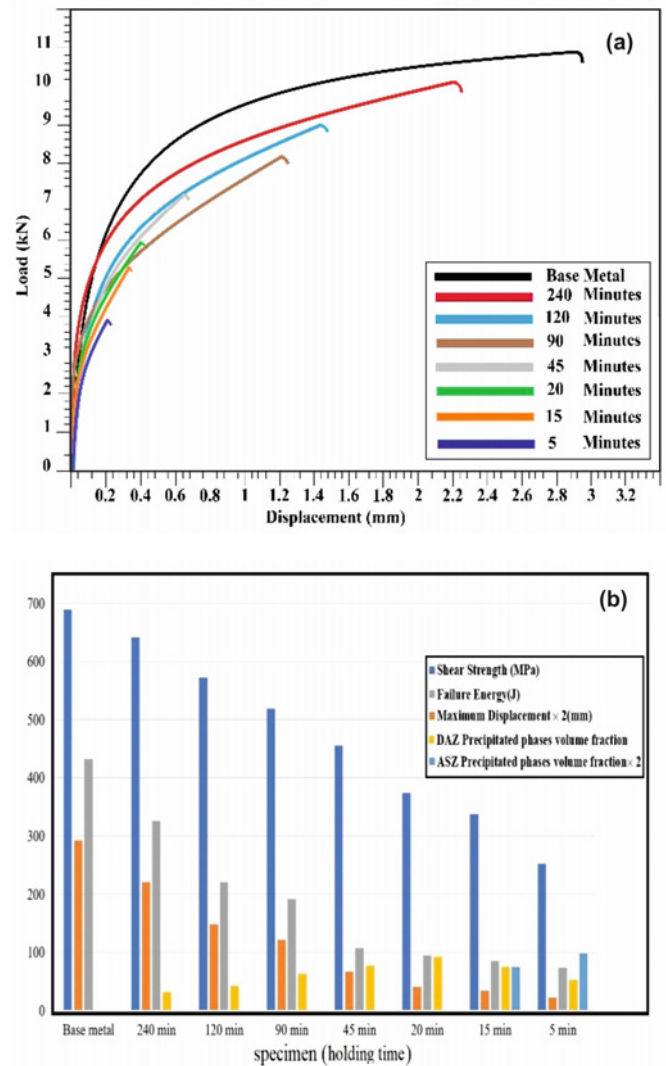
Fig. 15. (a) Load-displacement curves obtained for the shear tests applied to the base metal and all the diffusion brazed specimens at different holding times and (b) shear strength (MPa), maximum displacement (mm), failure energy (J), DAZ and ASZ precipitate phases volume fraction.

in Fig. 15, the maximum shear strength of 642 MPa belongs to the diffusion brazed specimen with a holding time of 240 min, and the lowest shear strength belongs to the diffusion brazed specimen with a holding time of 5 min. The shear strength of the 240 min holding time specimen reached 93 % of the shear strength of the base metal. Table 8 shows the shear strength of the specimens with the failure energy. Some researchers [18, 36] presented the reverse relationship between the width of the ASZ and the shear strength during the diffusion brazing of Inconel 718 superalloy. This subject was also observed in this study. By increasing the holding time to 20 min, the isothermal solidification was completed (the ASZ disappeared),

By increasing the holding time, the grain size of the interlayer was raised. This grain size change can also be observed in the base metal [35].

T a b l e 8. Shear strength, failure energy, and maximum displacement of the different holding times specimens and base metal

Specimen	Base metal	240 min	120 min	90 min	45 min	20 min	15 min	5 min
Shear strength (MPa)	690	642	572	519	455	373	338	252
Maximum displacement (mm)	2.92	2.21	1.48	1.21	0.66	0.41	0.33	0.22
Failure energy (J)	432	326	221	192	107	94	85	73
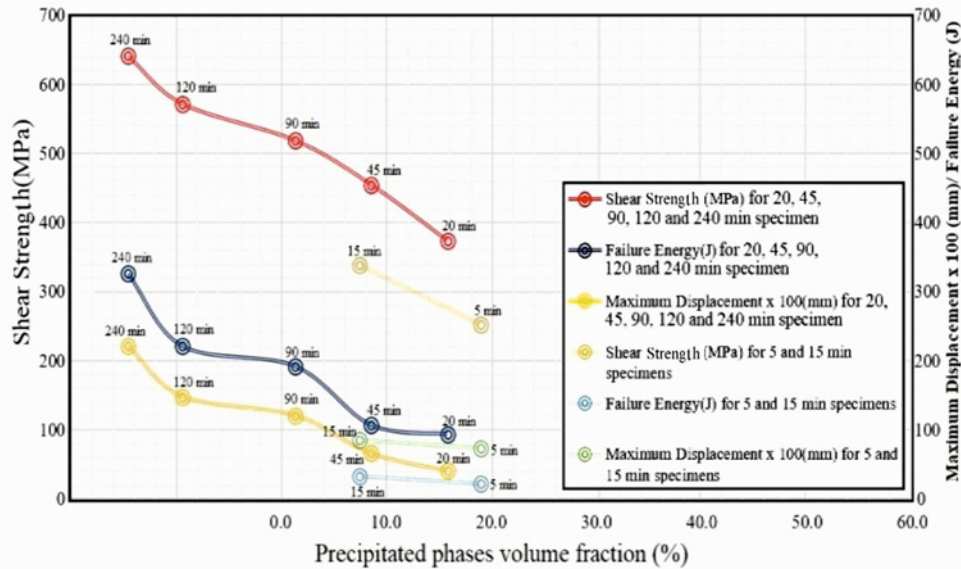
Fig. 16. Effect of all precipitate phases volume fraction (DAZ for 20, 45, 90, 120, and 240 min and ASZ for 15 and 5 min specimens) on the shear strength, failure energy, and maximum displacement of the different holding times specimens.

and the shear strength was promoted. Bridges et al. reported a similar increase in the shear strength by completing the isothermal solidification [37]. As can be seen, the shear strength of the specimens increased with increasing holding time. The energy required to fail the specimens, such as the shear strength, increased by increasing holding time. The study of the failure site of the specimens shows that in the case of specimens held at 5 and 15 min, which did not complete the isothermal solidification, the failure occurred from the bonding center and the ASZ region, and in other specimens that completed the isothermal solidification the failure occurred from the boundary between the ISZ and DAZ area, DAZ area and the boundary between the DAZ and base metal.

According to the Fig. 16, investigation of shear strength changes with volume fraction of precipitated phases in a DAZ and SAZ areas indicates that, in general, shear strength promoted with increasing holding time and simultaneously by reduction of volume fraction of precipitates in DAZ zone for 20, 45, 90, 120, and 240 min specimens and in ASZ zone for 5 and 15 min specimens, this phenomenon is also seen in the amount of failure energy and maximum displacement.

Simultaneously, increasing the time reduced the

volume fraction and morphology of the precipitates. Reducing the amount of precipitation and moving the precipitates deformation process towards spheroidizing improved mechanical properties and gotten closer to the base metal properties [38].

Some studies reported increased ductility with an increscent amount of boron in Ni-based superalloys [39, 40]. These studies gave evidence for the segregation of boron along the grain boundaries. In the diffusion brazing process, the completion of isothermal solidification, the occurrence of solid-state diffusion, and the formation of boride particles with uniform distribution are the main reasons for such an increase in ductility [41].

3.4. Microhardness evaluation

The hardness distribution in the bonding area can be employed to analyze and appraise the effect of secondary phases and the meager homogeneity on the mechanical properties of TLP joints [30]. The results of the Vickers microhardness distribution over the half joint area of the diffusion braze corresponding to different holding times are shown in Fig. 18. The hardness was measured at a distance of 5 μm, from the

Fig. 17. Effect of holding time on the thicknesses of ASZ and DAZ.

Fig. 18. Microhardness distribution over the half joint area of the bonds with different holding times indicates the hardness in ASZ, ISZ, DAZ, and BM areas.
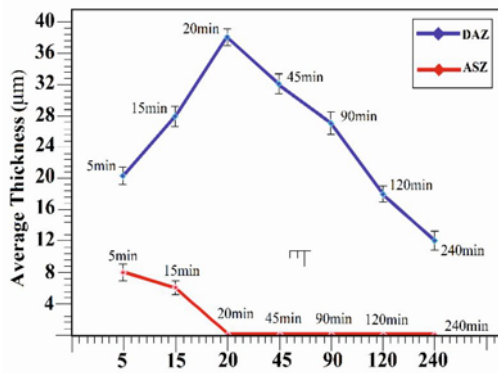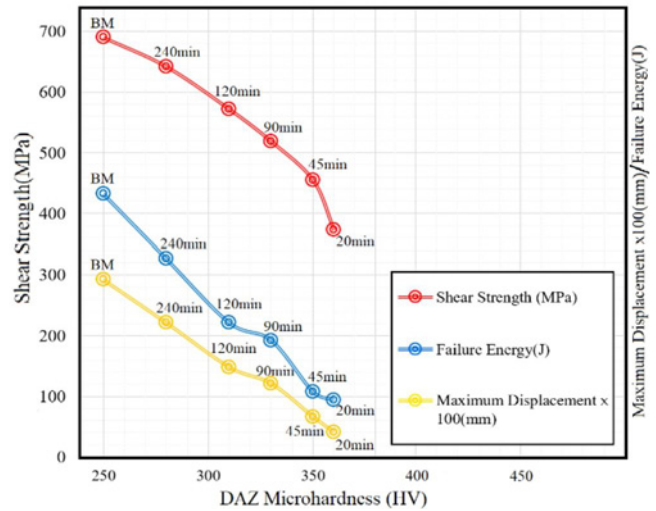
Fig. 19. Effect of DAZ microhardness on the shear strength, failure energy, and maximum displacement of the completed isothermal solidification step specimens.

DAZ zone due to the further dissolution of precipitated phases such as borides and carbides, and the ISZ hardness of the specimens by increasing holding times is close to that of the base metal; this can be relative to the higher interdiffusion between the bonding zone and the base metal. The effect of holding time on the thicknesses of ASZ and DAZ is shown in Fig. 17. As can be seen in Fig. 18, up to 20 min holding time as the long-distance diffusion of the elements into the base metal decreased, the density of the boride precipitates in the DAZ and width of DAZ increased and led to a decrease in the hardness in this region, but by holding for longer times, the rate of dissolution of precipitated phases increased, and the concentration of carbides and borides in the DAZ area decreased. Eventually, by increasing holding times, the hardness profile of the diffusion brazed joints became more uniform. The dominant hardening mechanism in the ISZ is a solid solution hardening mechanism controlled by the interdiffusion of solute elements between the base metal and interlayer [42].

Figure 19 simultaneously shows the relationship between the microhardness of the DAZ region and the shear strength, failure energy, and maximum displacement for specimens in which the isothermal solidification stage was completed. In the given bonding specimens from 20 to 240 min with increasing holding time, the hardness of the DAZ area decreased. The reason for the reduction of the hardness of the DAZ region in accordance with the results of Table 7 and the width of the DAZ region (Fig. 17) is the reduction of precipitated phase density (reduction of volume fraction) decrease in the width of the DAZ region and change the morphology of sedimentary particles [19, 33]. As seen in Fig. 19, the mechanical properties of the spec-

center of the interlayer to a few micrometers inside the base metal (15 points). Figure 18 shows the width of different bonding zones and the microhardness. The brittle and hard (Mo, Cr, Ni)-rich boride precipitates are attributed to an increase in the hardness in the center of the interlayer. As shown in Figs. 4–6, by increasing the holding time to 20 min, the joint region is erased from the hard and brittle centerline phases, and the ASZ is wholly removed; simultaneously, the hardness peak in the DAZ area can be seen, and as the holding time increases, the peak of hardness decreases in size and becomes closer to the base metal. This occurred with the reduction of the width of the

T a b l e 9. Chemical composition (at.%) of the particles on the fracture surfaces of the specimen diffusion brazed at 15 min (Fig. 20b)

Element	Cr	Co	Mo	C	B	Fe	Si	Ni	Probable phases
A	19.98	0.31	19.13	1.57	47.89	4.16	0.21	7.16	$(Mo,Cr)B$
B	43.88	0.42	0.02	1.25	52.14	1.66	0.01	1.14	$Cr B$
C	4.12	0.05	0.01	1.78	23.97	1.78	0.02	67.15	Ni_3B
D	0.81	0.02	0.03	0.72	0.01	0.63	32.40	65.43	Ni_2Si
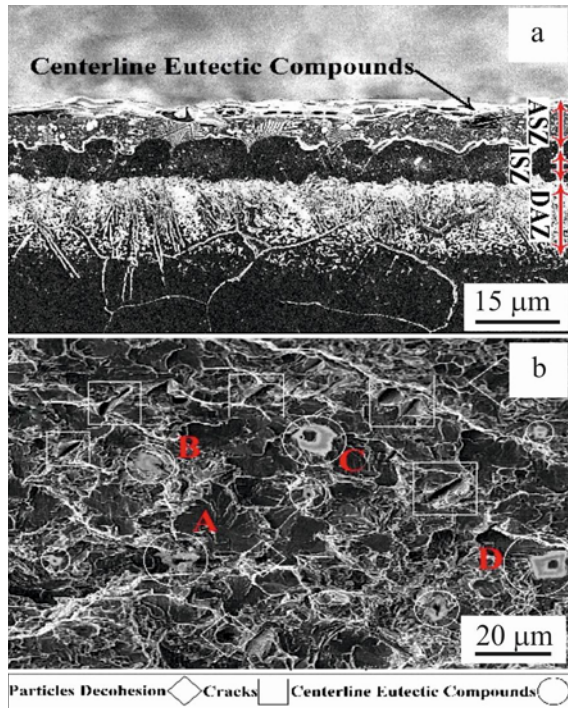
Fig. 20. The SEM images of the fractured diffusion brazed specimens at 15 min holding time: (a) SEM images of a polished cross-section showing the fracture path through the centerline eutectic compound in ASZ and (b) the SEM images illustrating the fracture surface morphology.

Fig. 21. XRD spectrum of the fracture surface of the 15 min holding time specimen.

imens increased with increasing holding time and, at the same time, reduced the hardness of the DAZ region [38].

3.5. Fracture morphology

Figure 20 shows the SEM images of the fractured diffusion brazed specimens at 15 min holding time. As shown in Fig. 20a, in the specimen diffusion brazed at 15 min, the fracture occurred exactly from the center of the bonding area, and the path of the eutectic precipitated ASZ phase. Figure 20b shows the fracture morphologies of the failure surface. This fracture morphology shows a semi-cleavage morphology, indicating a non-ductile fracture. Table 9 shows the EPMA spot test results for identifying the composition of the remained particles on the fracture surface. Point A

is mainly composed of (Mo-Cr)-rich borides, whereas point B is composed of chromium-rich borides, point C is nickel-rich boride (Ni_3B), and point D is Ni--rich silicide (Ni_2Si). The composition of these points is compatible with the phase compositions shown in Fig. 11. The XRD spectrum of the fracture surface of this specimen, which is shown in Fig. 21, confirms the accuracy of the type of mentioned formed phases in Table 9. Since the penetration of MPD elements such as B and Si in this specimen was not completed and there is a high concentration of this element in the middle of the interlayer, the presence of large amounts of borides and silicide phases is normal. Therefore, the fracture planes created in the vicinity of coarse boride particles caused brittle and cleavage failure characteristics and micro cracks. The intrinsic brittleness and pre-cracked structure result from low shear strength, maximum displacement, and failure energy, creating a rapid fracture.

Figure 22 shows the SEM images of the fractured diffusion brazed specimens at 45 min holding time, where the boundary between the ISZ and DAZ areas was the preferential site for crack propagation due to the presence of the borides and carbides. This fracture is brittle, and cracks are formed through carbides in grain boundaries. Table 10 shows the EPMA spot test results for identifying the composition of the remained particles in the fracture surface; Point A is composed of (Mo-Cr)-rich borides; Fig. 22b shows a mixture of

Table 10. Chemical composition (at.%) of the particles on the fracture surfaces of the specimen diffusion brazed at 45 min (Fig. 22b)

Element	Cr	Co	Mo	C	B	Fe	Si	Ni	Probable phases
A	26.74	0.18	19.33	1.53	45.75	2.95	0.03	2.67	$(Mo, Cr) B$
B	25.93	0.56	31.98	12.54	0.51	9.21	–	16.31	$(Ni,Mo,Cr,Fe)_6C$
C	38.82	0.78	27.12	19.15	0.58	6.96	–	6.11	$(Ni,Mo,Cr,Fe)_{23}C_6$
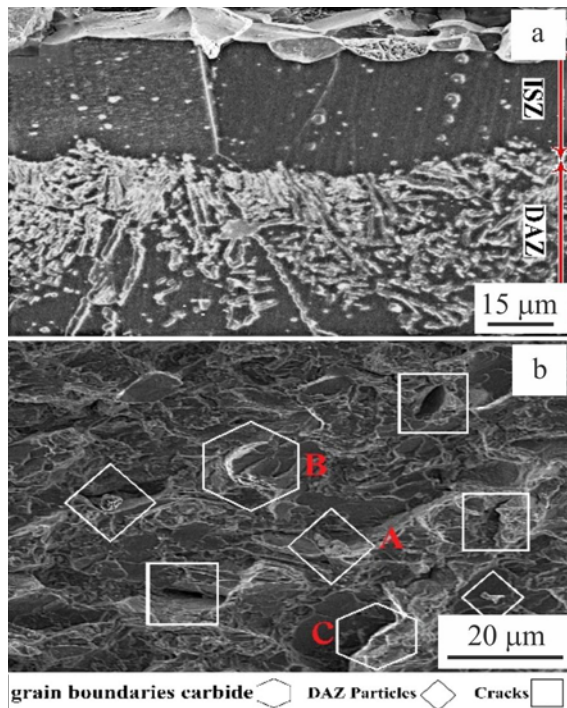
Fig. 22. The SEM images of the fractured diffusion brazed specimens at 45 min holding time: (a) SEM images of a polished cross-section showing the fracture path through the boundary between the ISZ and DAZ areas, and (b) the SEM images illustrating the fracture surface morphology.
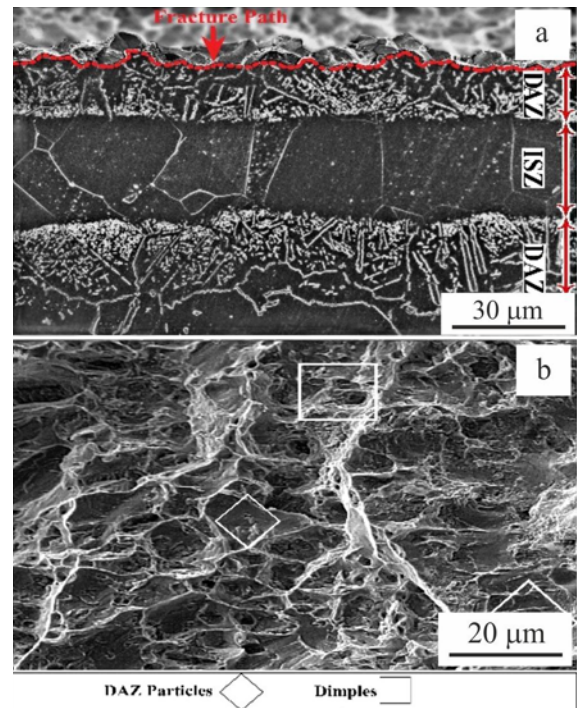
Fig. 24. The SEM images of the fractured specimen diffusion brazed at 240 min holding time: (a) SEM images of a polished cross-section showing the fracture path through the boundary between the DAZ and base metal areas, and (b) the SEM images illustrating the fracture surface morphology.
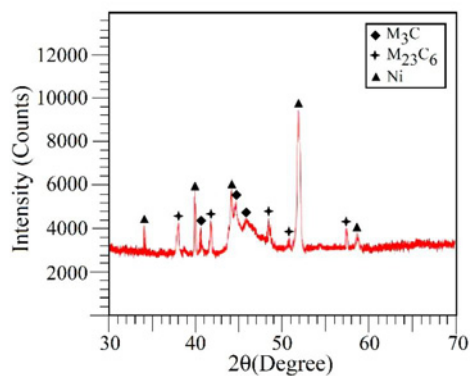
Fig. 23. XRD spectrum of the fracture surface of the 45 min holding time specimen.

granular and intergranular fracture facets. The boride particles are a source of intergranular fracture. The boride particles denote the site of crack nucleation. As can be seen in Table 10, Points B and C are complex carbides of $(Ni,Mo,Cr,Fe)_6C$ and $(Ni,Mo,Cr,Fe)_{23}C_6$. These carbides are responsible for granular fracture in the boundary between the ISZ and DAZ areas. It is concluded that the low shear strength and failure energy are attained when the most carbides are in grain boundaries. The XRD spectrum of the fracture surface of this specimen, which is shown in Fig. 23, confirms the accuracy of the type of mentioned formed phases in Table 10.

The fractured diffusion brazed specimen at 240 min holding time is shown in Fig. 24. The fracture path in this specimen is through the boundary between the

DAZ and base metal areas. After 20 min, by increasing the holding time, the ASZ region disappeared, and due to the diffusion of MPD elements to the base metal, the homogenization of DAZ decreased, but by promoting holding time, the width of the DAZ zone decreased by the solution of precipitate particles such as borides and carbides; therefore, effective factors of stress concentration decreased, and the shear strength increased [12, 43]. The fracture surface morphology shows a mixture of ductile and intergranular fractures. The ductile fracture has a high number of coarse dimples. The DAZ particles are visible in the depth of some dimples. The ductile fracture stems from the dimple formation mechanism in the strain discontinuity places. Often these discontinuities can be a second phase or precipitates [44]. The fracture surface of this specimen is a mixture of coarse dimples and cellular fracture. Brittle and ductile fracture characteristics can be seen in the cellular fracture mode [45]. Conspicuously, after completing isothermal solidification, when hard and brittle intermetallic compounds appear in the soft matrix (DAZ area) with the increase in the holding time, the precipitates become rounded, and their density decreases; as a result, at the same time, the probability of ductile failure with coarse dimples and the possibility of cellular structure increase. In this situation, the boride particles are surrounded by the soft matrix of the base metal, therefore, under applied stress, the matrix is deformed, and the cellular structure is created around the cracked particles due to the matrix plastic deformation [35].

4. Conclusions

The diffusion brazing of Nicrofer 5520 superalloy specimens was performed successfully at 1120 °C for seven different holding times of 5, 15, 20, 45, 90, 120, and 240 min using a 30 μm thick Ni-7%Cr 4.5%Si--3.1%B interlayer. The main findings of this study are as follows:

1. The isothermal solidification was completed for all the specimens after the holding time of 20 min, and the ASZ area was removed entirely. Before 20 min holding time, non-equilibrium eutectic phases were observed at the centerline of the bonding zone. The observed eutectic phases contain Ni-rich borides, Ni-rich silicides, Cr-rich borides, and Mo-rich borides. With increasing the holding time, the diffusion of B from the interlayer into the base metal caused the precipitation of (Mo and Cr)-rich borides in the DAZ of the joints. In this situation, a huge amount of complex Cr-Ni-Mo-Fe carbides, as granular carbides, were observed in the DAZ area.

2. With increasing the holding time, causal changes were made in the width of the DAZ zone. Actually, up to 20 min holding time, the long-distance diffusion of

the elements into the base metal caused a decrease in the density of the boride precipitates in the DAZ and an increase in the width of the DAZ. By holding for longer times, the dissolution rate of precipitated phases increased, and the concentration of carbides and borides in the DAZ area and its width decreased.

3. The high microhardness values obtained in the centerline of the interlayer were due to the precipitations of hard and brittle eutectic phases in the ASZ area and the (Mo and Cr)-rich borides and complex Cr-Ni-Mo-Fe carbides in the DAZ. In the following, by holding for longer times, the microhardness of the joints became more uniform because of the disappearance of the centerline eutectic phases and the eventually decreasing amounts of the borides and carbides in the DAZ area.

4. The shear strength of the specimens, the energy required failing, and the maximum displacement increased with increasing the holding time. The highest shear strength (~ 642 MPa) was achieved for the specimen diffusion brazed at a 240 min holding time that was about 93 % of the base metal strength, and the lowest shear strength (~ 252 MPa) was achieved for the specimen diffusion brazed at a 5 min holding time because of exhibiting of ASZ in center of bonding zone.

5. In the specimen diffusion brazed at 15 min, the fracture occurred exactly from the center of the bonding area, and the path was from the ASZ precipitated eutectic phase. This fracture morphology showed semi-cleavage morphology, indicating a nonductile fracture. In the diffusion brazed specimens at 45 min holding time, a fracture occurred in the boundary between the ISZ and DAZ areas, which was the preferential site for crack propagation due to the presence of the borides and carbides. This fracture was brittle, and the cracks were formed through carbides formed in the grain boundaries. The fracture surfaces of the specimen diffusion brazed at 240 min holding time were a mixture of a ductile fracture with a high number of coarse dimples, an intergranular fracture, and a cellular fracture.

Acknowledgement

References

[1] F. Jalilian, M. Jahazi, R. A. L. Drew, Microstructure evolution during transient liquid phase bonding of Al-

loy 617, Metallography, Microstructure, and Analysis 2 (2013) 170-182.
https://doi.org/10.1007/s13632-013-0070-z

[2] K. Mo, G. Lovicu, H.-M. Tung, X. Chen, J. Stubbins, High Temperature Aging and Corrosion Study on Alloy 617 and Alloy 230, 18th International Conference on Nuclear Engineering 2010, pp. 323–332. ISBN 978-0-7918-4933-0
https://doi.org/10.1115/ICONE18-30207

[3] F. Jalilian, M. Jahazi, R. A. L. Drew, Microstructural evolution during transient liquid phase bonding of Inconel 617 using Ni-Si-B filler metal, Materials Science and Engineering A 423 (2006) 269–281.
https://doi.org/10.1016/j.msea.2006.02.030

[4] H. Esmaeili, S. E. Mirsalehi, A. Farzadi, Vacuum TLP bonding of Inconel 617 superalloy using Ni-Cr-Si-Fe-B filler metal: Metallurgical structure and mechanical properties, Vacuum 152 (2018) 305–311.
https://doi.org/10.1016/j.vacuum.2018.03.048

[5] W. F. Gale, D. A. Butts, Transient liquid phase bonding, Science and Technology of Welding & Joining 9 (2004) 283–300.
https://doi.org/10.1179/136217104225021724

[6] S. Hadibeyk, B. Beidokhti, S. A. Sajjadi, Effect of bonding time and homogenization heat treatment on the microstructure and mechanical properties of the transient liquid phase bonded dissimilar GTD-111/FSX-414 TLP superalloys, Journal of Alloys and Compounds 731 (2018) 929–935.
https://doi.org/10.1016/j.jallcom.2017.10.105

[7] V. Jalilvand, H. Omidvar, M. R. Rahimipour, H. R. Shakeri, Influence of bonding variables on transient liquid phase bonding behavior of nickel based superalloy IN-738LC, Materials & Design (1980-2015) 52 (2013) 36–46.
https://doi.org/10.1016/j.matdes.2013.05.042

[8] M. Khakian, S. Nategh, S. Mirdamadi, Effect of bonding time on the microstructure and isothermal solidification completion during transient liquid phase bonding of dissimilar nickel-based superalloys IN738LC and Nimonic 75, Journal of Alloys and Compounds 653 (2015) 386–394.
https://doi.org/10.1016/j.jallcom.2015.09.044

[9] V. Jalilvand, H. Omidvar, H. R. Shakeri, M. R. Rahimipour, A study on the effect of process parameters on the properties of joint in TLP-bonded Inconel 738LC superalloy, Metallurgical and Materials Transactions B 44 (2013) 1222–1231.
https://doi.org/10.1007/s11663-013-9883-z

[10] V. Jalilvand, H. Omidvar, H. R. Shakeri, M. R. Rahimipour, Microstructural evolution during transient liquid phase bonding of Inconel 738LC using AMS 4777 filler alloy, Materials Characterization 75 (2013) 20–28.
https://doi.org/10.1016/j.matchar.2012.10.004

[11] F. Arhami, S. E. Mirsalehi, Microstructural evolution and mechanical properties evaluation of IN-939 bonds made by isothermal solidification of a liquated Ni-Cr-B interlayer, Metallurgical and Materials Transactions A 49 (2018) 6197–6214.
https://doi.org/10.1007/s11661-018-4918-3

[12] J. K. Kim, H. J. Park, D. N. Shim, D. J. Kim, Effect of bonding parameters on microstructural characteristics during TLP bonding of directionally solidified Ni-based superalloy, Journal of Manufacturing Processes

30 (2017) 208–216.
https://doi.org/10.1016/j.jmapro.2017.09.024

[13] W. F. Gale, E. R. Wallach, Microstructural development in transient liquid-phase bonding, Metallurgical Transactions A 22 (1991) 2451–2457.
https://doi.org/10.1007/BF02665011

[14] Standard Test Method for Microindentation Hardness of Materials, West Conshohocken, 2017, p. 40.

[15] A. Y. Shamsabadi, R. Bakhtiari, G. Eisaabadi B., TLP bonding of IN738/MBF20/IN718 system, Journal of Alloys and Compounds 685 (2016) 896–904.
https://doi.org/10.1016/j.jallcom.2016.06.185

[16] A. Doroudi, A. Dastgheib, H. Omidvar, The bonding temperature effect of the diffusion brazing Inconel 625 superalloy on the microstructure changes, corrosion resistance, and mechanical properties, Journal of Manufacturing Processes 53 (2020) 213–222.
https://doi.org/10.1016/j.jmapro.2020.02.005

[17] O. A. Ojo, L. Richards, M. Chaturvedi, Isothermal solidification during transient liquid phase bonding of Inconel 738 superalloy, Science and Technology of Welding & Joining 9 (2004) 532–540.
https://doi.org/10.1179/174329304X8702

[18] M. Pouranvari, A. Ekrami, A. H. Kokabi, Effect of bonding temperature on microstructure development during TLP bonding of a nickel base superalloy, Journal of Alloys and Compounds 469 (2009) 270–275.
https://doi.org/10.1016/j.jallcom.2008.01.101

[19] F. Arhami, S. E. Mirsalehi, A. Sadeghian, Effect of bonding time on microstructure and mechanical properties of diffusion brazed IN-939, Journal of Materials Processing Technology 265 (2019) 219–229.
https://doi.org/10.1016/j.jmatprotec.2018.10.021

[20] L. X. Zhang, Z. Sun, Q. Xue, M. Lei, X. Y. Tian, Transient liquid phase bonding of IC10 single crystal with GH3039 superalloy using BNi2 interlayer: Microstructure and mechanical properties, Materials & Design 90 (2016) 949–957.
https://doi.org/10.1016/j.matdes.2015.11.041

[21] A. Malekan, M. Farvizi, S. E. Mirsalehi, N. Saito, K. Nakashima, Effect of bonding temperature on the microstructure and mechanical properties of Hastelloy X superalloy joints bonded with a Ni-Cr-B-Si-Fe interlayer, Journal of Manufacturing Processes 47 (2019) 129–140.
https://doi.org/10.1016/j.jmapro.2019.09.030

[22] M. Pouranvari, A. Ekrami, A.H. Kokabi, Solidification and solid state phenomena during TLP bonding of IN718 superalloy using Ni-Si-B ternary filler alloy, Journal of Alloys and Compounds 563 (2013) 143–149.
https://doi.org/10.1016/j.jallcom.2013.02.100

[23] O. A. Idowu, N. L. Richards, M. C. Chaturvedi, Effect of bonding temperature on isothermal solidification rate during transient liquid phase bonding of Inconel 738LC superalloy, Materials Science and Engineering: A 397 (2005) 98–112.
https://doi.org/10.1016/j.msea.2005.01.055

[24] M. Pouranvari, A. Ekrami, A. H. Kokabi, Microstructure evolution mechanism during post-bond heat treatment of transient liquid phase bonded wrought IN718 superalloy: An approach to fabricate boride-free joints, Journal of Alloys and Compounds 723 (2017) 84–91.   https://doi.org/10.1016/j.jallcom.2017.06.206

[25] M. A. Arafin, M. Medraj, D. P. Turner, P. Bocher, Transient liquid phase bonding of Inconel 718 and Inconel 625 with BNi-2: Modeling and experimental investigations, Materials Science and Engineering: A 447 (2007) 125–133. https://doi.org/10.1016/j.msea.2006.10.045

[26] O. A. Idowu, O.A. Ojo, M.C. Chaturvedi, Microstructural study of transient liquid phase bonded cast INCONEL 738LC superalloy, Metallurgical and Materials Transactions A 37 (2006) 2787–2796. https://doi.org/10.1007/BF02586111

[27] G. Marchese, G. Basile, E. Bassini, A. Aversa, M. Lombardi, D. Ugues, P. Fino, S. Biamino, Study of the microstructure and cracking mechanisms of Hastelloy X produced by laser powder bed fusion, Materials 11 (2018) 106. https://doi.org/10.3390/ma11010106

[28] B. Zhang, G. Sheng, Y. Jiao, Z. Gao, X. Gong, H. Fan, J. Zhong, Precipitation and evolution of boride in diffusion affected zone of TLP joint of Mar-M247 superalloy, Journal of Alloys and Compounds 695 (2017) 3202–3210. https://doi.org/10.1016/j.jallcom.2016.11.306

[29] M.-C. Liu, G.-M. Sheng, H.-J. He, Y.-J. Jiao, Microstructural evolution and mechanical properties of TLP bonded joints of Mar-M247 superalloys with Ni-Cr-Co-W-Ta-B interlayer, Journal of Materials Processing Technology 246 (2017) 245–251. https://doi.org/10.1016/j.jmatprotec.2017.03.021

[30] D. Amiri, S. A. Sajjadi, R. Bakhtiari, A. Kamyabi-Gol, The role of TLP process variables in improvement of microstructure and mechanical properties in TLP joints of GTD-111/Ni-Cr-Fe-B-Si/GTD-111 system, Journal of Manufacturing Processes 32 (2018) 644–655. https://doi.org/10.1016/j.jmapro.2018.03.036

[31] M. Pouranvari, A. Ekrami, A. H. Kokabi, Effect of the bonding time on the microstructure and mechanical properties of a transient-liquid-phase bonded IN718 using a Ni-Cr-B filler alloy, Materiali in Tehnologije 47 (2013) 593–599.

[32] A. Malekan, M. Farvizi, S. E. Mirsalehi, N. Saito, K. Nakashima, Holding time influence on creep behavior of transient liquid phase bonded joints of Hastelloy X, Materials Science and Engineering A 772 (2020) 138694. https://doi.org/10.1016/j.msea.2019.138694

[33] A. Sadeghian, S. E. Mirsalehi, F. Arhami, A. Malekan, N. Saito, K. Nakashima, Effect of bonding time on dissimilar Transient Liquid Phase (TLP) bonding of IN939 to IN625 superalloys: Microstructural characterization and mechanical properties, Metallurgical and Materials Transactions A 52 (2021) 1526–1539. https://doi.org/10.1007/s11661-021-06176-x

[34] A. Sadeghian, F. Arhami, S. E. Mirsalehi, Phase formation during dissimilar transient liquid phase (TLP) bonding of IN939 to IN625 using a Ni-Cr-Fe-Si-B interlayer, Journal of Manufacturing Processes 44 (2019) 72–80. https://doi.org/10.1016/j.jmapro.2019.05.027

[35] A. Malekan, M. Farvizi, S. E. Mirsalehi, N. Saito, K. Nakashima, Influence of bonding time on the transient liquid phase bonding behavior of Hastelloy X using Ni-Cr-B-Si-Fe filler alloy, Materials Science and Engineering A 755 (2019) 37–49. https://doi.org/10.1016/j.msea.2019.03.124

[36] A. Doroudi, A. Ebrahimzadeh Pilehrood, M. Mohebinia, A. Dastgheib, A. Rajabi, H. Omidvar, Effect of the isothermal solidification completion on the mechanical properties of Inconel 625 transient liquid phase bond by changing bonding temperature, Journal of Materials Research and Technology 9 (2020) 10355–10365. https://doi.org/10.1016/j.jmrt.2020.07.015

[37] D. Bridges, R. Xu, A. Hu, Microstructure and mechanical properties of Ni nanoparticle-bonded Inconel 718, Materials & Design 174 (2019) 107784. https://doi.org/10.1016/j.matdes.2019.107784

[38] F. Arhami, S. E. Mirsalehi, A. Sadeghian, M. H. Johar, The joint properties of a high-chromium Ni-based superalloy made by diffusion brazing: Microstructural evolution, corrosion resistance and mechanical behavior, Journal of Manufacturing Processes 37 (2019) 203–211. https://doi.org/10.1016/j.jmapro.2018.11.025

[39] P. Kontis, H. A. M. Yusof, S. Pedrazzini, M. Danaie, K. L. Moore, P. A. J. Bagot, M. P. Moody, C. R. M. Grovenor, R. C. Reed, On the effect of boron on grain boundary character in a new polycrystalline superalloy, Acta Materialia 103 (2016) 688–699. https://doi.org/10.1016/j.actamat.2015.10.006

[40] D. Wu, T. Yao, D. Li, S. Lu, Effect of boron on the tensile and creep properties of a newly developed Ni-Fe-based weld metal, Materials Science and Engineering: A 731 (2018) 21–28. https://doi.org/10.1016/j.msea.2018.06.027

[41] S. Shakerin, H. Omidvar, S. E. Mirsalehi, The effect of substrate's heat treatment on microstructural and mechanical evolution of transient liquid phase bonded IN-738 LC, Materials & Design 89 (2016) 611–619. https://doi.org/10.1016/j.matdes.2015.10.003

[42] M. Pouranvari, A. Ekrami, A. H. Kokabi, TLP bonding of cast IN718 nickel based superalloy: Process–microstructure–strength characteristics, Materials Science and Engineering: A 568 (2013) 76–82. https://doi.org/10.1016/j.msea.2013.01.029

[43] A. Doroudi, A. Shamsipur, H. Omidvar, M. Vatanara, Effect of transient liquid phase bonding time on the microstructure, isothermal solidification completion and the mechanical properties during bonding of Inconel 625 superalloy using Cr-Si-B-Ni filler metal, Journal of Manufacturing Processes 38 (2019) 235–243. https://doi.org/10.1016/j.jmapro.2019.01.019

[44] D. A. Butts, W. F. Gale, Transient liquid phase bonding of Gamma Met PX: Microstructure and mechanical properties, Materials Science and Technology 24 (2008) 1492–1500. https://doi.org/10.1179/174328407X236535

[45] D. Hull, Fractography: Observing, Measuring, and Interpreting Fracture Structure Topography, Cambridge University Press, Cambridge, 1999. ISBN: 9780521646840.